Colloids and Surfaces B: Biointerfaces 105 (2013) 199–206

Contents lists available at SciVerse ScienceDirect

Colloids and Surfaces B: Biointerfaces

journal homepage: www.elsevier.com/locate/colsurfb

Coalesced chitosan activated carbon composite for batch and fixed-bed adsorption of cationic and anionic dyes

M. Auta, B.H. Hameed*

School of Chemical Engineering, Engineering Campus, Universiti Sains Malaysia, 14300 Nibong Tebal, Penang, Malaysia

ARTICLE INFO

Article history:
Received 18 July 2012
Received in revised form
10 December 2012
Accepted 12 December 2012
Available online 31 December 2012

Keywords:
Adsorption
Kinetics
Thermodynamics
Equilibrium
Composite
Reusability

ABSTRACT

A renewable waste tea activated carbon (WTAC) was coalesced with chitosan to form composite adsorbent used for waste water treatment. Adsorptive capacities of crosslinked chitosan beads (CCB) and its composite (WTAC-CCB) for Methylene blue dye (MB) and Acid blue 29 (AB29) were evaluated through batch and fixed-bed studies. Langmuir, Freundlich and Temkin adsorption isotherms were tested for the adsorption process and the experimental data were best fitted by Langmuir model and least by Freundlich model; the suitability of fitness was adjudged by the Chi-square (χ^2) and Marquadt's percent standard deviation error functions. Judging by the values of χ^2, pseudo-second-order reaction model best described the adsorption process than pseudo-first-order kinetic model for MB/AB29 on both adsorbents. After five cycles of adsorbents desorption test, more than 50% WTAC-CCB adsorption efficiency was retained while CCB had <20% adsorption efficiency. The results of this study revealed that WTAC-CCB composite is a promising adsorbent for treatment of anionic and cationic dyes in effluent wastewaters.

© 2012 Elsevier B.V. All rights reserved.

1. Introduction

Veneration of our pristine environment is geometrically diminishing due to human non-adherence to environmental laws in their quest for technological advancement. Pollutants such as dyes, heavy metals, pesticides and pharmaceutical wastes are alien to groundwater and rivers thereby impacting negatively on the ecosystem. Membrane separation techniques, precipitation, ion-exchange, electrochemical, adsorption and oxidation processes are among the science and engineering approaches toward waste water management but they have their limitations toward efficiency. Adsorption techniques for removal of dye pollutants from industrial effluents are highly effective and economical [1]. For some decades now, it is the prime technique under investigation or exploration for remediation, restoration and sustainability of our environment from dyes pollutants [2,3].

Chitosan, a deacetylated product of biopolymer chitin has found applications in various fields such as cosmetics, paper, textile and food processing industries, medicine, agriculture, photography, chromatographic separations, waste water treatment and solid state batteries [4,5]. Its versatility in various fields is due to some of its enviable properties such as biodegradability, biocompatibility, functional groups, low toxicity, renewability, large molecular weight, particle size, density, viscosity and so on [6]. Specifically, its attractive characteristics in adsorption include: presence of hydroxyl (—OH), amino ($—NH_2$) groups, flexibility of its chains, among others. However, chitosan has some chemical and mechanical weaknesses which include formation of colloid like solution when in contact with water, dissolution in acids, formation of gel in aqueous solution, susceptibility to biochemical and microbiological degradation and low surface area [7,8]. Functionalization (grafting) and crosslinking helps to improve its chemical stability while its mechanical strength is improved through physical modifications which include granulation and impregnation of its powder on a support [9–12].

Various forms of chitosan composite adsorbents have been prepared with a view to improving its applicability in adsorption processes. The adsorbents include magnetic chitosan [12–14], chitosan activated carbon [15], chitosan clay [16], quartenarized chitosan [9], polyvinyl alcohol chitosan [17] and others. Much work has been reported on dyes adsorption using chitosan and activated carbon separately, but this research is based on enhancement of adsorption of dyes using chitosan activated carbon composite.

This research is aimed at investigating the synergetic effect between waste tea activated carbon and chitosan on removal of cationic and anionic dyes through batch and column adsorption processes. To achieve the aforementioned goals, effect of pH, cross-linking, initial concentration, temperature, bed height, flow rate, thermodynamic, kinetics and isothermal studies were analyzed.

* Corresponding author. Tel.: +60 45996422; fax: +60 45941013.
E-mail address: chbassim@eng.usm.my (B.H. Hameed).

0927-7765/$ – see front matter © 2012 Elsevier B.V. All rights reserved.
http://dx.doi.org/10.1016/j.colsurfb.2012.12.021

2. Materials and methods

2.1. Materials

Chitosan flakes (molecular weight, MW = 400,000, degree of deacetylation, DD = 90%) were supplied by Hunza Pharmaceutical Sdn Bhd., Nibong Tebal, Malaysia. Methylene Blue (MB) and Acid Blue 29 (AB29) were supplied by Sigma–Aldrich chemicals while all other chemicals of analytical grade were purchased from Merck Chemicals Company, all in Malaysia. Waste from tea was obtained from cafeteria of Engineering Campus, Universiti Sains Malaysia.

2.2. Preparation of adsorbents

Waste tea activated carbon (WTAC) was prepared as previously reported [18]. Chitosan flakes (2 g) were dissolved in 100 mL of 0.7 M CH_3COOH and stirred (125 rpm) for 5 h at 30 °C. The dissolved molten chitosan solution was added dropwise into 0.067 M NaOH solution to form beads. The chitosan beads were crosslinked with 125 mL of 0.1 M epichlorohydrin (ECH) solution and then placed in water-bath shaker (130 rpm) at 50 °C for 6 h. The crosslinked chitosan beads (CCB) were finally freeze dried and packaged for usage.

Waste tea activated carbon-chitosan composite beads (WTAC-CCB) were prepared by adding 1 g of WTAC to an equivalent chitosan solution and stirred for 5 h. The mixture was added dropwise into 0.067 M NaOH solution to form beads and kept overnight. The beads were then crosslinked similarly as CCB. The composite beads (WTAC-CCB) were freeze-dried and packaged for usage.

2.3. Characterization of CCB and WTAC-CCB adsorbents

The pH point of zero charge (pHzpc) of CCB and WTAC-CCB was carried out using solid addition method as described in our previous study [18]. The functional groups present in chitosan (CH), CCB and WTAC-CCB were determined using Fourier transformed infrared spectroscopy (FTIR) and the surface morphology of WTAC-CCB before and after adsorption were examined using scanning electron microscopy (SEM).

The FTIR analysis of the substances (CH, CCB and WTAC-CCB) was carried out using a Perkin Elmer Spectrum GX Infrared Spectrometer with resolution of 4 cm^{-1}, in the range of 4000–400 cm^{-1}. The analytical KBr and the substances were dried overnight in different ovens set at 110 and 50 °C prior to the analysis. The dried substances were ground into fine particles and mixed with the KBr in a ratio of 20:1 (KBr/substance) for disc technique method of FTIR analysis.

Surface morphology of WTAC-CCB before and after adsorption of MB and AB29 were examined using scanning electron microscope (Model EMJEOL-JSM6301-F) with an Oxford INCA/ENERGY-350 microanalysis system.

2.4. Adsorption studies

2.4.1. Effect of solution pH on MB/AB29 adsorption by both CCB and WTAC-CCB

The effect of pH on adsorption experiment was carried out as preliminary study to determine the suitable pH for adsorption of MB/AB29 on both CCB and WTAC-CCB. The study was conducted in a set of 250 mL Erlenmeyer flasks containing 200 mg/L of MB/AB29 initial concentration and 0.10 g of the adsorbent beads (1–2 mm). The flasks were placed in an isothermal water-bath shaker (130 rpm) at 30 °C for 1200 min (CCB) and 300 min (WTAC-CCB). A pH 3–12 of the adsorbate solution was used which were adjusted using either NaOH or H_2SO_4 solution. The pH value was measured using pH meter (Model Delta 320, Mettler Toledo, China). The amount of the adsorbate adsorbed at equilibrium q_e (mg/g) was evaluated using Eq. (1):

$$q_e = \frac{(C_o - C_e)V}{W} \quad (1)$$

where C_o and C_e (mg/L) are the liquid-phase concentration of the MB/AB29 at initial and at equilibrium, respectively; V (L) is the volume of the solution; and W (g) is the mass of the dried adsorbent.

2.5. Kinetics and batch equilibrium studies

Kinetics and equilibrium adsorption experiments were conducted in a set of 250 mL Erlenmeyer flasks containing 100 mL of MB/AB29 solutions at various initial concentrations of 50–350 mg/L. Added to each flask was 0.1 g (1–2 mm) of the adsorbent (CCB/WTAC-CCB) and the pH of the mixture was adjusted using either NaOH or H_2SO_4, pH 10 was used for MB adsorption on CCB, pH 7 for MB on WTAC-CCB and pH 3 for AB29 adsorption on both CCB and WTAC-CCB. The flasks were then placed in an isothermal water-bath shaker (130 rpm) at 30 °C and a set time (1000 min for CCB adsorbing MB, 200 min for WTAC-CCB adsorbing MB, 200 min for CCB adsorbing AB29 and 100 min for WTAC-CCB adsorbing AB29) to reach equilibrium. Prior to dynamic equilibrium attainment, the residual adsorbate concentration was determined using UV–vis spectrophotometer (Shimadzu UV/vis 1601 spectrophotometer, Japan) at maximum wavelength of 668 for MB and 602 for AB29. The entire process was repeated by varying water-bath shaker temperature to 40 and 50 °C.

The amount of the adsorbate adsorbed on the adsorbent at time t, q_t (mg/g) was calculated using a mass balance equation (2):

$$q_t = \frac{(C_o - C_t)V}{W} \quad (2)$$

where C_o and C_t (mg/L) are the liquid-phase concentration of the MB/AB29 at initial and at any time t, respectively; V (L) is the volume of the solution; and W (g) is the mass of the dried adsorbents. The reliability of the adsorption process was checked by repeating the entire experiment three times, this lead to determination of standard error (SD) of the set of different data generated.

Effect of inorganic salts (NaCl, $NaHCO_3$ and Na_2SO_4) on removal of dyes was investigated. Concentrations of salts used in the study were 0.1, 0.5 and 1.0 M and dye concentration was maintained at 200 mg/L. Adsorption experiments were carried out in accordance with equilibrium studies.

2.6. Desorption studies

The recovered adsorbents (0.1 g) from 250 mL Erlenmeyer flasks containing 100 mL (200 mg/L initial concentration) used for batch adsorption studies were rinsed slightly with deionized water and then air dried. The dried adsorbents were placed in 250 mL flasks containing 100 mL deionized water and the pH was adjusted to 10 and 3 for AB29 and MB, respectively. The flasks were placed in isothermal water-bath shaker with similar conditions as obtained in the adsorption study, for desorption experiment. After desorption, the adsorbents were slightly rinsed with water, air dried and ready for the next adsorption experiment. The cycle was repeated five times. Desorption efficiency of the CCB/WTAC-CCB adsorbent was determined as:

$$\text{Desorption efficiency } (\%) = \frac{M_d V_d}{W \times q_e \times 100} \times 100 \quad (3)$$

where M_d (mg/L) is the concentration of MB/AB29 desorbed from pre-adsorbed CCB/WTAC-CCB adsorbent, V_d (L) is the volume of the solution used for desorption, W (g) is the mass of the pre-adsorbed adsorbent, q_e (mg/g) is the amount of the pre-adsorbed adsorbate on the adsorbent and 100 is the initial volume (mL) of the adsorbate

where the adsorbent was recovered. Two sets of freshly recovered adsorbents were used to verify the desorption studies data obtained.

2.7. Fixed-bed column experiment

A jacketed Pyrex glass tube with internal diameter 1.2 cm and 19.5 cm length was employed as the fixed-bed column. It has a stainless steel sieve positioned at the bottom to support a layer of glass beads. A predetermined mass of WTAC-CCB (1–2 mm) was measured into the column for bed heights of 2.5, 3.6 and 4.5 cm which were corresponding to 0.7, 1.0 and 1.25 g, respectively. Uniform flow of the system was improved by placing ample quantity of glass beads which also retarded fluidization of the system. Variance of flow rates 5, 8 and 10 mL/min was used to impregnate the column with the dye solution through upward flow aided by a peristaltic pump (Master-flex, Cole-Parmer Instrument Co.) for various initial influent concentrations of 50, 100 and 200 mg/L. A pipe loop system of an isothermal water-bath set at 30 °C was used to regulate the temperature of the system. The residual dye in the outlet flow was determined at intervals of time with the aid of UV–vis spectrophotometer (Shimadzu UV/vis 1601, Japan) at maximum wavelength, λ_{max} = 668 for MB and λ_{max} = 602 for AB29. The entire fixed-bed study was repeated three times to check probable flaws of the experiment.

2.7.1. Fixed-bed column data analysis

Breakthrough curves, a valuable aspect of fixed-bed studies shows the mass transfer zone which gives information on the characteristics of adsorbate on adsorbent [19]. The breakthrough sorption profiles were obtained by plots of C_t (mg/L) or C_t/C_o versus V_t (mL) or t (min), taking C_t as the effluent concentration, C_o influent concentration, V_t treated effluent volume and t as the service time. Volume of the treated effluent, V_t was calculated using Eq. (4):

$$V_t = Qt_e \tag{4}$$

where Q is the influent flow rate (mL/min) and t_e is the time at exhaustion (min).

At every influent concentration with respect to the set flow rate, amount of MB/AB29 adsorbed was measured by computing the area under the plot through integration of adsorbed concentration expressed as C_{ad} ($C_{ad} = C_o - C_t$) (mg/L) for a given time t (min). The amount adsorbed in the fixed-bed column [q_{total} (mg)] was evaluated using Eq. (5) [20]:

$$q_{total} = \frac{QA}{1000} = \frac{Q}{1000}\int_{t=0}^{t=t_{total}} C_{ad}\,dt \tag{5}$$

where t_{total}, Q and A are the total flow time (min), volumetric flow rate (mL/min) and the area under the breakthrough curve, respectively. Equilibrium uptake ($q_{eq(exp)}$) (mg/g) is determined as:

$$q_{eq(exp)} = \frac{q_{total}}{m} \tag{6}$$

where m (g) is the amount of adsorbent in the fixed-bed column. The amount of dye passed into the column – W_{total} (mg) is determined as:

$$W_{total} = \frac{C_o Q t_{total}}{1000} \tag{7}$$

Percentage of dye removed is the quotient of the maximum capacity of the column (q_{total}) divided by the total amount of dye sent to the column (W_{total}) expressed as:

$$R = \frac{q_{total}}{W_{total}} \times 100 \tag{8}$$

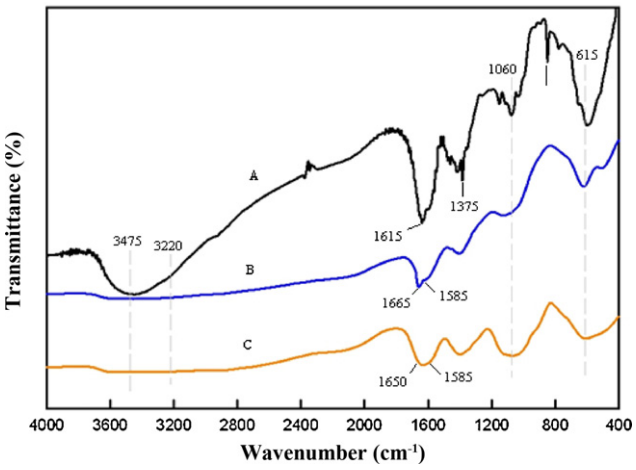

Fig. 1. FTIR spectra of (A) WTAC-CCB, (B) CCB and (C) CH.

3. Results and discussion

3.1. Characterization of CCB and WTAC-CCB

The pHzpc of WTAC [18], CCB and WTAC-CCB were 7.4, 5.6 and 6.8, respectively. At these points, surfaces of the adsorbents had zero net charge; this is the point at which they exhibited amphoteric characteristics. pHzpc provides information on the ability of surfaces (adsorbents) to adsorb ions from solution [21].

The SEM morphological identification micrographs of the adsorbent before and after adsorption were taken (figure not shown). The micrographs for both MB and AB29 of WTAC-CCB after adsorption had their surfaces covered with irregular adhered substances which were suspected to be the adsorbate molecules; unlike the structure of the adsorbent before adsorption which had a clear plain surface.

The FTIR spectra of CH, CCB and WTAC-CCB were taken to identify the functional groups responsible for the binding mechanism between the adsorbent and adsorbate (MB/AB29). Adsorption band width around 3475–3220 cm^{-1} which disclosed presence of O—H and N—H functional groups were of high intensity on WTAC-CCB than on CH and CCB spectra; the peaks are characteristic features of WTAC [18]. Common adsorption band of CH around wave numbers 1650 and 1060 cm^{-1} were altered after crosslinking when compared with CCB spectrum. Adsorption peak at 1665 cm^{-1} on CCB spectrum signified presence of imine moiety formed during chitosan crosslinking reaction, appearance of an absorption peak at this wavenumber confirmed crosslinking reaction of chitosan [22]. The stretching of O—H and N—H functional groups and the presence of unattached amino groups from the cross-linked chitosan due to N—H group's scissor from the primary amine were shown on the peaks at wavenumbers 1650 and 1585 cm^{-1}; these are common chitosan and cross-linked chitosan features [13]. It has been reported that a distinct band at 1585 cm^{-1} was as a result of bending vibration of aliphatic secondary amine emanating from reaction of $-NH_2$ and ECH [23]. A large cluster of functional groups such as C=O, C—O and C=C were found at wavenumber intervals of 1375–615 cm^{-1}. The presence of these numerous functional groups in the WTAC-CCB composite also contributed to the adsorption of MB/AB29. Increase in the intensity of peaks around wave numbers of 615, 1615, 3655–3220 cm^{-1} where N—H were located, was attributed to the synergetic effect of the constituents of the composite, as compared with the less pronounced peaks on similar wave numbers of spectrum for WTAC [18]. The spectra for CH, CCB and WTAC-CCB composite are shown in Fig. 1.

3.2. Effect of solution pH on MB/AB29 adsorption

One of the key parameters of describing surface chemistry of an adsorbent is its pH [24]. A pH 2–10 was used to study its effect on adsorption of MB/AB29 on CCB and WTAC-CCB. Higher adsorption of AB29 was observed at lower pH 2–4, while at pH 8–10 the poorest adsorption was noted (figure not shown). In the acidic medium, populated protons attracted negatively charged molecules of AB29 through electrostatic attraction as opposed to repulsive activities experienced at higher pH due to the presence of some OH^- radicals, this is comparable to reports on methyl orange adsorption on cross-linked magnetic chitosan composite [13] and adsorption of acid dyes by chitosan beads adsorbents [25]. The high adsorption observed at low pH of the composite adsorbent, affirmed improvement on its adsorptive properties as compared with chitosan beads adsorbent; as a result, pH 3 was selected for adsorption of AB29 on WTAC-CCB composite. Similarly, in strong acidic solution, competition between protons and cationic molecules of MB hindered its adsorption activities on the surface of WTAC-CCB. However, at elevated pH values, good adsorption of MB onto the adsorbent surface was observed. Thus, pH 7 was adopted for further adsorption studies of MB.

3.3. Effect of initial concentration on MB/AB29 adsorption on CCB and WTAC-CCB

Initial concentrations of MB/AB29 from 50 to 350 mg/L were varied to study the effect of concentration on the adsorption process. Adsorption uptake increased with increase in initial concentration and faster equilibrium was achieved at lower concentrations (figure not shown). This was attributed to availability of sufficient vacant active sites at lower concentrations which had limited adsorbates molecules to occupy on both CCB and WTAC-CCB. The superfluous unsaturated vacant sites present in the adsorption process at low concentrations transformed into lower adsorption uptake of pollutant from solution. Similar scenario observed has been reported [26,27].

3.4. Effect of inorganic salts on dye removal

Effect of salts on uptake of dyes result is shown in Fig. 2a. Removal of MB and AB29 by CCB and WTAC-CCB were not much affected (84–97%) and the order of influence was $SO_4^{2-} > HCO_3^- > Cl^-$ for Na_2SO_4, $NaHCO_3$ and NaCl, respectively. The sulphate anions impact was attributed to their interaction with protonated amino groups on chitosan reducing polymer solubility and availability of the amino groups [28]. Lower impact of $NaHCO_3$ and NaCl on dye removal has been reported [29,30].

3.5. Adsorption equilibrium isotherm

Adsorption equilibrium isotherm was studied using Langmuir (9) [31], Freundlich (10) [32] and Temkin (11) [33] models. The non-linear form of the isotherms models are given as:

$$q_e = \frac{q_m C_e b}{(1 + bC_e)} \quad (9)$$

$$q_e = K_F C_e^{1/n} \quad (10)$$

$$q_e = B \ln(K_T C_e) \quad (11)$$

where C_e (mg/L) is the equilibrium concentration of MB/AB29 adsorbed and q_e (mg/g) is the experimental adsorption capacity of MB/AB29; Langmuir constants q_m (mg/g) and b (L/g) are the monolayer adsorption capacity and affinity of adsorbent toward adsorbate, respectively. Freundlich constants K_F ((mg/g)(L/mg)$^{1/n}$) and n (dimensionless), gives information on the extent of adsorption and the degree of nonlinearity between the adsorption and the solution concentration, respectively. The inverse of n ($1/n$), evaluates the adsorption intensity. Temkin constant k_T (L/mg), relay information on the equilibrium binding constant correlating the maximum binding energy while $B = RT/b_T$, where R is universal gas constant (8.314 J/(mol K)), T (K) is absolute temperature and b_T (J/mol) is related to heat of adsorption.

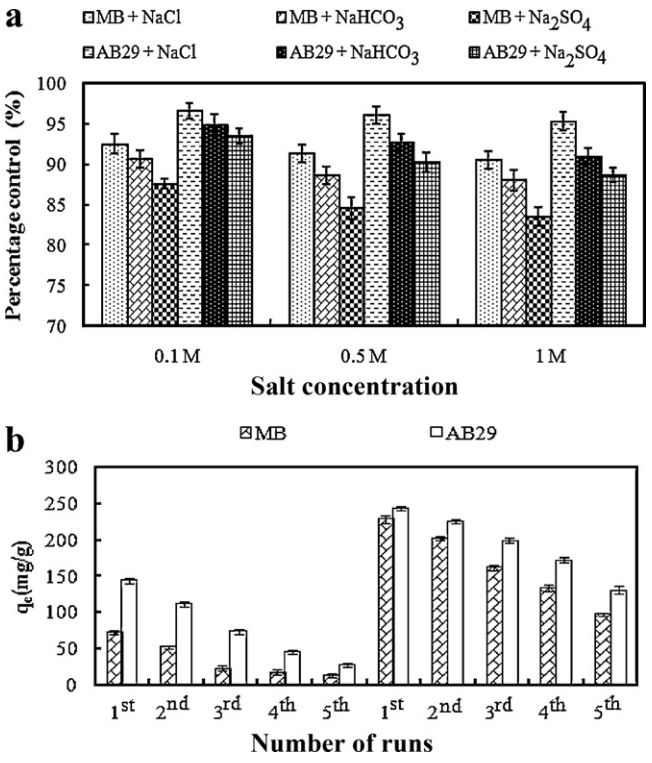

Fig. 2. (a) Effect of inorganic salts on adsorption of MB and AB29 by WTAC-CCB. (b) Adsorption capacities of CCB and WTAC-CCB for five runs of desorption and regeneration experiments for MB/AB29 adsorption at 30 °C and 200 mg/L; values are the mean of $n = 3$ (mean ± SD).

Evaluation of the results of model fitting to the adsorption of MB/AB29 showed that Langmuir isotherm model best described the adsorption processes for both CCB and WTAC-CCB adsorbents; this was based on the high values of correlation coefficients R^2. The R^2 values for Freundlich and Temkin models isotherms could not be used to determine the best fit due to their inconsistent trend [34].

To study the applicability of models equation fitness to the experimental data and validate the best fit, error functions such as chi-square (χ^2) and Marquadt's percent standard deviation (MPSD) equations were used which are given as Eq. (12) and (13), respectively:

$$\chi^2 = \frac{\sum(q_{e,exp} - q_{e,cal})}{q_{e,exp}} \quad (12)$$

$$\text{MPSD} = 100 \times \left[\sqrt{\frac{1}{n-p} \sum_{i=1}^{p} \left[\frac{\sum \left(q_{e,exp} - q_{e,cal} \right)}{q_{e,exp}} \right]_i^2} \right] \quad (13)$$

where $q_{e,exp}$ is the experimental data and $q_{e,cal}$ is the calculated data. The error functions were used to determine error distribution between the predicted and experimental values of the isotherm models. The lower the error value the better the conformity between the examined values. Therefore, the results of the error functions further justified the best fitness of Langmuir

Table 1
Langmuir, Freundlich and Temkin isotherm models constants, correlation coefficients, SD ($n = 3$ for each point), and error function parameters of MB/AB29 adsorption on CCB and WTAC-CCB.

Isotherms	Parameters	CCB						WTAC-CCB					
		MB			AB29			MB			AB29		
		30 °C	40 °C	50 °C	30 °C	40 °C	50 °C	30 °C	40 °C	50 °C	30 °C	40 °C	50 °C
Langmuir	q_m(mg/g)	103.64	172.67	234.5	193.4	265.3	376.9	197.3	268.9	388.1	345.1	446.2	596.4
	b (L/g)	0.076	0.004	0.019	0.016	0.015	0.099	0.455	0.126	0.199	0.033	0.241	0.402
	R^2	0.987	0.979	0.992	0.990	0.986	0.982	0.977	0.992	0.984	0.993	0.994	0.998
	χ^2	1.278	0.016	0.173	1.809	3.206	0.455	0.104	0.575	0.316	0.243	0.193	0.544
	MPSD	1.078	0.066	1.208	1.227	1.092	0.164	2.062	3.465	2.004	1.03	1.884	2.140
	SD ($n = 3$)	3.12	1.46	1.24	1.11	0.88	1.21	2.22	3.45	2.03	0.63	1.18	2.48
Freundlich	K_F ((mg/g)(L/mg)$^{1/n}$)	2.764	6.218	13.94	7.72	8.17	27.18	17.88	29.92	42.45	23.15	39.89	88.21
	$1/n$	0.832	0.737	0.509	0.617	0.693	0.503	0.550	0.716	0.766	0.782	0.618	0.559
	R^2	0.992	0.981	0.973	0.992	0.999	0.985	0.978	0.980	0.989	0.986	0.948	0.967
	χ^2	2.957	7.634	12.68	17.78	10.35	12.22	10.73	9.461	3.422	0.354	4.946	1.825
	MPSD	10.88	24.31	8.68	25.31	19.43	11.90	34.25	23.15	15.74	13.52	7.30	2.22
	SD ($n = 3$)	4.22	3.02	1.28	4.88	5.02	1.78	2.16	3.28	2.66	1.45	2.71	0.81
Temkin	k_T (L/mg)	12.71	16.35	15.72	39.38	45.80	32.45	41.12	38.88	39.39	65.90	54.43	22.83
	b_T (kJ/mol)	0.032	0.085	0.008	0.753	0.587	0.502	0.626	0.342	0.333	0.606	0.321	0.115
	R^2	0.907	0.969	0.966	0.985	0.876	0.963	0.936	0.987	0.957	0.978	0.984	0.988
	χ^2	2.957	7.634	12.68	12.32	3.045	8.470	0.765	1.226	1.027	6.131	4.883	9.383
	MPSD	2.116	3.242	4.543	6.243	1.782	7.585	2.036	4.447	2.855	8.17	5.56	3.22
	SD ($n = 3$)	0.687	1.005	0.072	4.336	0.768	3.211	2.01	2.56	1.99	0.87	1.32	2.05

isotherm to the adsorption processes. The χ^2 and MPSD values for Freundlich model for MB/AB29 adsorption on CCB and WTAC-CCB were larger than those of both Temkin and Langmuir, signifying poor fitness of the experimental data to the model. Results for isotherms models parameters and their validation with χ^2 and MPSD for CCB and WTAC-CCB are summarized in Table 1.

Crosslinked chitosan beads adsorbent had the lowest adsorption capacity for both MB and AB29 adsorbates. This can be attributed to limited access to adsorption sites of chitosan due to its low surface area [35]. But attainment of equilibrium position was faster with WTAC-CCB. At 30 °C, equilibrium of adsorption of MB and AB29 on CCB were attained in 600 and 110 min, respectively, while 80 and 40 min were the time taken to attain equilibrium for MB and AB29 adsorption on WTAC-CCB, respectively.

The power of synergy on efficiency of WTAC-CCB adsorbent through enhancement of chitosan stability in low acid concentration as well as its surface area manifested positively. The high surface area, porous and multifunctional groups of WTAC [18,36] compositely bound with the functional groups (amino —NH_2 and hydroxyl —OH) of chitosan [13]. The WTAC-CCB composite was durable at low acid concentrations and had higher reusability efficiency than the individual effects of the composites constituents.

3.6. Adsorption kinetics on MB/AB29 adsorption by CCB and WTAC-CCB

Two kinetic models pseudo-first-order and pseudo-second-order equations were used to determine the model that best described adsorption of MB/AB29 on CCB and WTAC-CCB. The non-linear form of pseudo-first order (14) [37] and pseudo-second-order (15) [38] equations are:

$$q_t = q_e(1 - e^{-k_1 t}) \quad (14)$$

$$q_t = \frac{k_2 q_e^2 t}{(1 + k_2 q_e t)} \quad (15)$$

where q_e and q_t (mg/g), are the amount of MB/AB29 adsorbed on CCB/WTAC-CCB at equilibrium and at any time t (h), respectively; k_1 (h^{-1}) and k_2 (g/(mg h)) are the rate constants for pseudo-first and pseudo-second order of adsorption. Parameters of the two models obtained from plots of q_t against t and the experimental conditions are summarized in Table 2. The results showed that pseudo-second-order kinetic model best described both MB and AB29 adsorption on CCB and WTAC-CCB more than the first-order-kinetic model. This was based on pseudo-second-order model least χ^2 values. This is similar to the report on adsorption of reactive dye on cross-linked chitosan/oil palm ash composite beads [39].

3.7. Thermodynamics studies

The adsorption of MB/AB29 on both CCB and WTAC-CCB increased with corresponding temperature increase, this signified endothermic adsorption process. The enthalpy (ΔH), entropy (ΔS) and Gibbs free energy (ΔG) of the adsorption processes were calculated from the following equations:

$$\Delta G = -RT \ln K_o \quad (16)$$

$$\ln K_o = \frac{\Delta G}{RT} = \frac{\Delta S}{R} - \frac{\Delta H}{RT} \quad (17)$$

where R is the universal gas constant (8.314 J/Kmol), T the absolute temperature (K) and K_o the distribution coefficient expressed as $K_o = C_e$ (adsorbent)/C_e (solution).

Adsorption on CCB and WTAC-CCB of MB/AB29 were spontaneous and the degree of dispersion of the processes increased with temperature. This is as a result of the negative values of ΔG and positive values of ΔS obtained from the processes (table not shown). The results showed that the adsorption processes for MB/AB29 adsorption on both CCB and WTAC-CCB were endothermic and also dominated by enthalpy activities rather than entropy ($\Delta H > T\Delta S$) [40,41].

3.8. Desorption studies

The reusability test according to Section 2.6 was repeated five times and the results are summarized in Fig. 2. The desorption activities was due to electrostatic repulsion which occurred when the pH of the adsorbate solution was adjusted, similar observation has been reported [42]. The desorption efficiency of CCB adsorbent dropped drastically after the second cycle while WTAC-CCB efficiency was above 50% after the fifth cycle.

Table 2
Parameters, SD ($n = 3$ for each point) and χ^2 of pseudo-first and second-order reaction models for MB and AB29 adsorption on CCB and WTAC-CCB.

Adsorbent	Dye	Temp. (°C)	q_{exp} (mg/g)	Pseudo-first-order parameters					Pseudo-second-order parameters				
				k_1 (h^{-1})	q_{cal} (mg/g)	R^2	χ^2	SD, $n = 3$	k_2 ($\times 10^4$ g/(mg h))	q_{cal} (mg/g)	R^2	χ^2	SD, $n = 3$
CCB	MB	30	30.11	0.004	19.31	0.96	6.04	3.02	1.42	26.18	0.99	0.59	0.96
		40	37.61	0.006	28.93	0.94	2.60	2.76	1.20	39.73	0.99	0.11	1.78
		50	49.45	0.008	50.80	0.99	0.04	2.14	1.05	68.39	0.97	5.24	3.14
	AB29	30	94.86	0.066	84.11	0.97	1.37	5.22	10.0	93.36	0.99	0.02	2.65
		40	103.9	0.037	88.41	0.99	2.73	3.54	21.2	93.48	0.98	0.58	4.88
		50	113.1	0.031	96.63	0.99	2.82	2.98	73.5	100.5	0.99	1.59	3.84
WTAC-CCB	MB	30	148.4	0.115	131.4	0.95	2.19	4.56	12.0	147.2	0.98	0.01	2.36
		40	155.8	0.191	138.8	0.98	2.08	3.24	24.0	150.1	0.99	0.22	2.87
		50	163.2	0.234	145.6	0.99	2.15	3.08	29.6	154.1	0.99	0.54	3.45
	AB29	30	166.7	0.173	153.6	0.98	1.12	4.73	17.7	164.9	0.99	0.02	1.08
		40	170.1	0.251	160.7	0.98	0.55	2.99	26.0	167.0	0.99	0.06	2.11
		50	173.8	0.576	161.0	0.99	1.01	2.12	151	174.8	0.99	0.01	2.67

3.9. Fixed-bed adsorption studies

3.9.1. Effect of MB/AB29 initial concentration

The MB/AB29 initial influent stream at 5 mL/min to a bed height of 3.6 cm had its concentration variations of 50, 100 and 200 mg/L. The prolonged breakthrough curves which showed treatment of large volume of the solution containing MB/AB29, was at 50 mg/L while at 200 mg/L, shorter stretch of the breakthrough curves signifying smaller dye solution treatment capability. The differences resulted due to smaller mass transfer of solutes in 50 mg/L and 200 mg/L having larger solute concentration. Exhaustion point was attained at 2220 and 900 min for 50 and 200 mg/L, respectively. Adsorption capacity of WTAC-CCB increased with solute concentration of 50, 100 and 200 mg/L corresponding to 160.45, 297.77, 376.72 and 410.13, 432.86, 531.07 mg/g for MB and AB29, respectively. This is in agreement with the expected trend [43]. The breakthrough curves for effect of initial influent concentration on adsorption of MB and AB29 are shown in Fig. 3.

3.9.2. Effect of influent flow rate on adsorption

The influent stream (50 mg/L) was set at different flow rates (5, 8 and 10 mL/min) into the column of bed depth 3.6 cm for MB/AB29 adsorption on WTAC-CCB. Better performance of the column was found at 8 mL/min with adsorption capacity of 196.96 mg/g for MB which was neither the slowest nor fastest flow-rate of the influent solution. Lower influent flow rate may contain insufficient

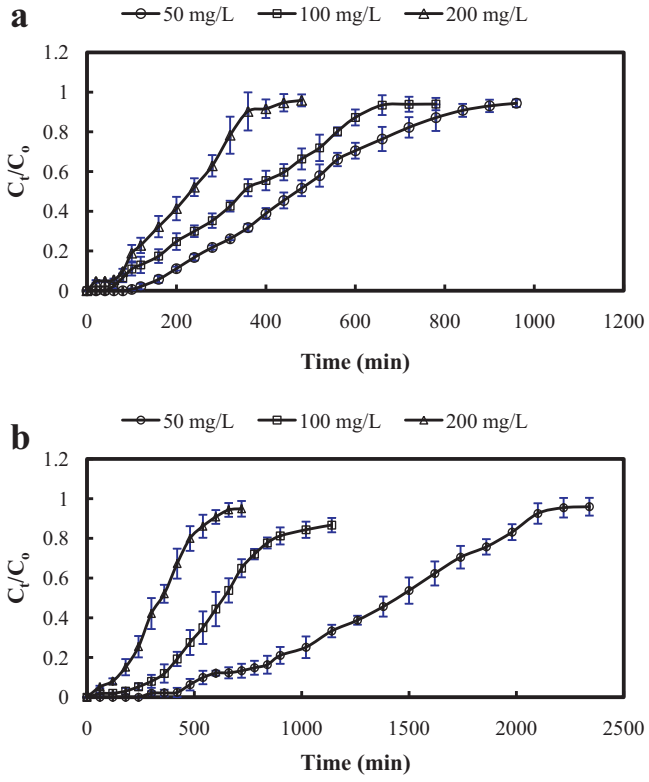

Fig. 3. Effect of concentration on (a) MB and (b) AB29 adsorption by WTAC-CCB adsorbent at bed height of 3.6 cm, 30 °C and 5 mL/min flow rate; plotted points are values of the mean of $n = 3$ (mean ± SD).

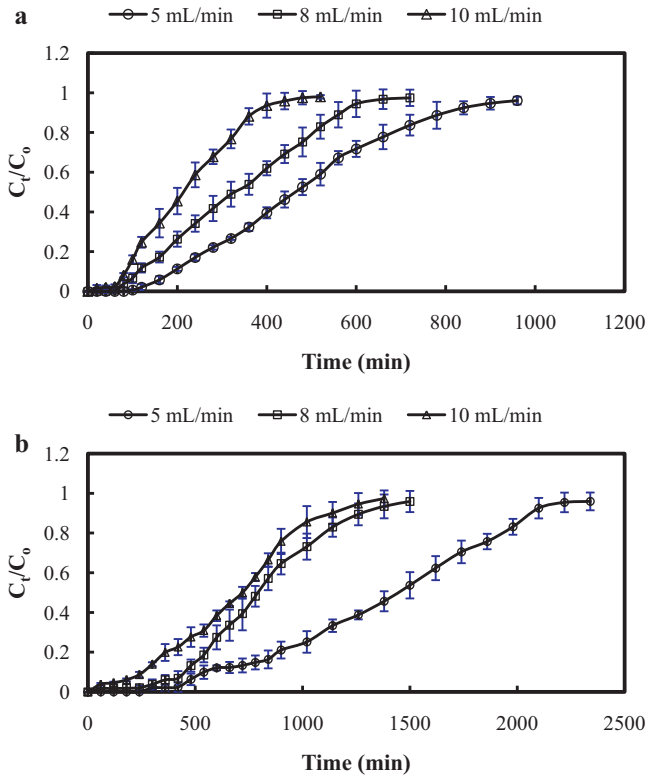

Fig. 4. Effect of solution flow rate on (a) MB and (b) AB29 adsorption by WTAC-CCB adsorbent at bed height of 3.6 cm, 30 °C and 50 mg/L concentration; plotted points are values of the mean of $n = 3$ (mean ± SD).

Table 3
Fixed-bed column study parameters and SD ($n = 3$ for each point) obtained at different inlet concentration, bed height and flow rates for adsorption of MB and AB29 by WTAC-CCB at 30 °C.

Dye	Concentration, C_o (mg/L)	Bed height, H (cm)	Flow rate, Q (mL/min)	q_{total} (mg)	$q_{eq(exp)}$ (mg/g)	SD ($n = 3$)
MB	50	2.5	5	89.56	127.94	5.36
	50	3.6	5	160.45	160.45	0.73
	50	4.5	5	204.06	163.25	1.67
	50	3.6	8	196.96	196.96	4.45
	50	3.6	10	194.78	194.78	7.09
	100	3.6	5	297.77	297.77	4.29
	200	3.6	5	376.72	376.72	3.77
AB29	50	2.5	5	234.49	334.99	4.31
	50	3.6	5	410.13	410.13	0.39
	50	4.5	5	526.53	421.22	1.28
	50	3.6	8	433.11	433.11	3.37
	50	3.6	10	495.15	495.15	5.64
	100	3.6	5	432.86	432.86	4.36
	200	3.6	5	531.07	531.07	3.18

MB solute (50 mg/L) to occupy the numerous vacant active sites of WTAC-CCB while inadequate residence time of solute in the column disallowing optimum adsorbate–adsorbent interaction may have attributed to lower capacity of adsorption; lower column utilization was observed at higher influent flow rates [26]. However, the best column performance for AB29 adsorption on WTAC-CCB with an adsorption capacity of 495.15 mg/g was found at the highest flow rate of 10 mL/min. Higher mass transfer and protonation of more amine group at pH 3 may have contributed to better adsorption observed. Fig. 4 shows the breakthrough profiles for effect of influent flow rate on MB/AB29 adsorbent on WTAC-CCB.

3.9.3. *Effect of WTAC-CCB bed depth on adsorption*

The effect of variation of service area of the column adsorption of MB/AB29 was studied by varying bed depths of 2.5, 3.6 and 4.5 cm at constant influent concentration and flow rate of 50 mg/L and 5 mL/min, respectively. Proportionality was established between the extension of breakthrough profiles and increase in bed depth. Increase in bed depth lead to extension of breakthrough and its exhaustion time. Higher mass of the adsorbent increased the number of the binding sites, larger service area for adsorption activities to take place and possibility of treating large volumes of effluent dye solution, whereas the reverse was the case at shorter bed depth. Axial dispersion was the characteristics of mass transfer activities at smaller bed depths due to insufficient adsorbate–adsorbent interaction within the limited contact period. Profiles of lower bed depths were steeper and shorter while those of the longer bed depth were prolonged. Similar observation on adsorption of reactive azo dye onto granular activated carbon has been reported [44]. Bed depth profiles for MB and AB29 are shown in Fig. 5 and their corresponding adsorption capacities are summarized in Table 3, respectively.

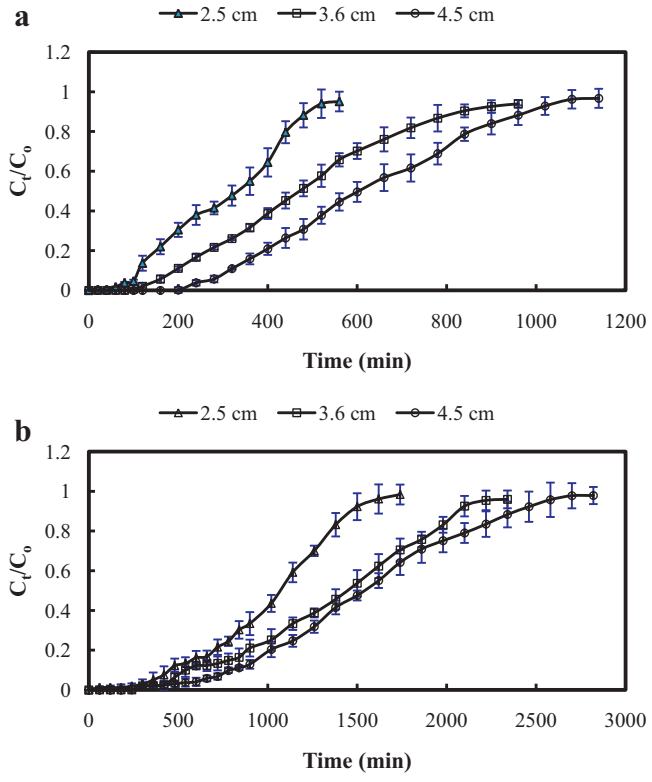

Fig. 5. Effect of bed height on (a) MB and (b) AB29 adsorption by WTAC-CCB adsorbent at 50 mg/L, 30 °C and 5 mL/min; plotted points are values of the mean of $n = 3$ (mean ± SD).

4. Conclusion

The reactivity of crosslinked WTAC-CCB created by inequality between intra and inter-particle forces as a result of its numerous functional groups on its surface indicated by the FTIR analysis, gave rapid adsorption of both MB and AB29. The adsorption by CCB/WTAC-CCB of MB/AB29 was spontaneous, endothermic and the experimental data were best described by pseudo-second-order reaction model. Adsorption activities were mostly on the monolayer surface with high adsorbate–adsorbent interaction as revealed by the isotherms models studies which were in accordance to fitness Langmuir, Temkin and Freundlich, respectively. The reusability test further distinguished the composite synergetic effect from their individual components adsorption capability. After five cycles of adsorbents desorption test, more than 50% WTAC-CCB adsorption efficiency was retained while CCB had <20% adsorption efficiency. The low pH 3 for adsorption of AB29 and the rate of adsorption of both MB and AB29 revealed that CCB and WTAC [18] mono-sorbent limitations were remediated by their combined effect.

Acknowledgement

Authors acknowledge the research grant provided by the Universiti Sains Malaysia under the Research University (RU) Schemes (Project No. 1001/PJKIMIA/814005) and (Project No. 1001/PJKIMIA/8045026).

References

[1] M. Toor, B. Jin, Adsorption characteristics, isotherm, kinetics, and diffusion of modified natural bentonite for removing diazo dye, Chem. Eng. J. 187 (2012) 79.

[2] M.A.M. Salleh, D.K. Mahmoud, W.A.W.A. Karim, A. Idris, Cationic and anionic dye adsorption by agricultural solid wastes: a comprehensive review, Desalination 280 (2011) 1.

[3] G. Crini, Non-conventional low-cost adsorbents for dye removal: a review, Bioresour. Technol. 97 (2006) 1061.

[4] P.K. Dutta, J. Dutta, V.S. Tripathi, Chitin and chitosan: chemistry, properties and applications, J. Sci. Ind. Res. 63 (2004) 20.

[5] A. Bansiwal, D. Thakre, N. Labhshetwar, S. Meshram, S. Rayalu, Fluoride removal using lanthanum incorporated chitosan beads, Colloids Surf. B: Biointerfaces 74 (2009) 216.

[6] V.R. Sinha, A.K. Singla, S. Wadhawan, R. Kaushik, R. Kumria, K. Bansal, S. Dhawan, Chitosan microspheres as a potential carrier for drugs, Int. J. Pharm. 274 (2004) 1.

[7] M.L.P. Dalida, A.F.V. Mariano, C.M. Futalan, C.C. Kan, W.C. Tsai, M.W. Wan, Adsorptive removal of Cu(II) from aqueous solutions using non-crosslinked and crosslinked chitosan-coated bentonite beads, Desalination 275 (2011) 154.

[8] M.Z. Elsabee, R.E. Morsi, A.M. Al-Sabagh, Surface active properties of chitosan and its derivatives, Colloids Surf. B: Biointerfaces 74 (2009) 1.

[9] M. Sarkar, P. Majumdar, Application of response surface methodology for optimization of heavy metal biosorption using surfactant modified chitosan bead, Chem. Eng. J. 175 (2011) 376.

[10] P. Mallika, A. Himabindu, D. Shailaja, Modification of chitosan towards a biomaterial with improved physico-chemical properties, J. Appl. Polym. Sci. 101 (2006) 63.

[11] W.S. Wan Ngah, L.C. Teong, M. Hanafiah, Adsorption of dyes and heavy metal ions by chitosan composites: a review, Carbohydr. Polym. 83 (2011) 1446.

[12] L. Fan, M. Li, Z. Lv, M. Sun, C. Luo, F. Lu, H. Qiu, Fabrication of magnetic chitosan nanoparticles grafted with β-cyclodextrin as effective adsorbents toward hydroquinol, Colloids Surf. B: Biointerfaces 95 (2012) 42.

[13] H.Y. Zhu, R. Jiang, L. Xiao, W. Li, A novel magnetically separable γ-Fe_2O_3/crosslinked chitosan adsorbent: preparation, characterization and adsorption application for removal of hazardous azo dye, J. Hazard. Mater. 179 (2010) 251.

[14] M. Monier, D.M. Ayad, D.A. Abdel-Latif, Adsorption of Cu(II), Cd(II) and Ni(II) ions by cross-linked magnetic chitosan-2-aminopyridine glyoxal Schiff's base, Colloids Surf. B: Biointerfaces 94 (2012) 250.

[15] A. Venault, L. Vachoud, C. Pochat, D. Bouyer, C. Faur, Elaboration of chitosan/activated carbon composites for the removal of organic micropollutants from waters, Environ. Technol. 29 (2008) 1285.

[16] L. Wang, A. Wang, Adsorption behaviors of Congo red on the N,O-carboxymethyl-chitosan/montmorillonite nanocomposite, Chem. Eng. J. 143 (2008) 43.

[17] X. Li, Z. Ye, Y. Li, Preparation of macroporous bead adsorbents based on poly(vinyl alcohol)/chitosan and their adsorption properties for heavy metals from aqueous solution, Chem. Eng. J. 178 (2011) 60.

[18] M. Auta, B.H. Hameed, Preparation of waste tea activated carbon using potassium acetate as an activating agent for adsorption of Acid Blue 25 dye, Chem. Eng. J. 171 (2011) 502.

[19] M.A. Martín-Lara, G. Blázquez, A. Ronda, I.L. Rodríguez, M. Calero, Multiple biosorption–desorption cycles in a fixed-bed column for Pb(II) removal by acid-treated olive stone, J. Ind. Eng. Chem. 18 (2012) 1006.

[20] S.D. Faust, O.M. Aly, Adsorption Processes for Water Treatment, Butterworth Publishers, 1987.

[21] N.A. Oladoja, I.A. Ololade, S.E. Olaseni, V.T. Olatujoye, O.S. Jegede, O. Agunloye, Synthesis of nano calcium oxide from a gastropod shell and the performance evaluation for Cr(VI) removal from aqua system, Ind. Eng. Chem. Res. 51 (2012) 639.

[22] N.K. Lazaridis, G.Z. Kyzas, A.A. Vassiliou, D.N. Bikiaris, Chitosan derivatives as biosorbents for basic dyes, Langmuir 23 (2007) 7634.

[23] J. Miao, L.-C. Zhang, H. Lin, An investigation into a novel kind of thin film composite nanofiltration membrane with sulfated chitosan as the active layer material, Chem. Eng. Sci. 87 (2013) 152.

[24] K.M. Smith, G.D. Fowler, S. Pullket, N.J.D. Graham, Sewage sludge-based adsorbents: a review of their production, properties and use in water treatment applications, Water Res. 43 (2009) 2569.

[25] K. Azlan, W.N. Wan Saime, K.L. Lai, Chitosan and chemically modified chitosan beads for acid dyes sorption, J. Environ. Sci. 21 (2009) 296.

[26] S. Hussain, H.A. Aziz, M.H. Isa, A. Ahmad, J. Van Leeuwen, L. Zou, S. Beecham, M. Umar, Orthophosphate removal from domestic wastewater using limestone and granular activated carbon, Desalination 271 (2011) 265.

[27] M. Anbia, S.A. Hariri, S.N. Ashrafizadeh, Adsorptive removal of anionic dyes by modified nanoporous silica SBA-3, Appl. Surf. Sci. 256 (2010) 3228.

[28] R. Salehi, M. Arami, N.M. Mahmoodi, H. Bahrami, S. Khorramfar, Novel biocompatible composite (chitosan–zinc oxide nanoparticle): preparation, characterization and dye adsorption properties, Colloids Surf. B: Biointerfaces 80 (2010) 86–93.

[29] A. Arunarani, P. Chandran, B.V. Ranganathan, N.S. Vasanthi, S. Sudheer Khan, Bioremoval of Basic Violet 3 and Acid Blue 93 by *Pseudomonas putida* and its adsorption isotherms and kinetics, Colloids Surf. B: Biointerfaces 102 (2013) 379–384.

[30] A. Szyguła, E. Guibal, M. Ruiz, A.M. Sastre, The removal of sulphonated azo-dyes by coagulation with chitosan, Colloids Surf. Physicochem. Eng. Aspects 330 (2008) 219–226.

[31] I. Langmuir, The constitution and fundamental properties of solids and liquids. Part 1. Solids, J. Am. Chem. Soc. 38 (1916) 2221.

[32] H.M.F. Freundlich, Over the adsorption in solution, J. Phys. Chem. 57 (1906) 385.

[33] M.J. Temkin, V. Pyzhev, Recent modifications to Langmuir isotherms, Acta Physiochim. USSR 12 (1940) 217.

[34] S. Azizian, B. Yahyaei, Adsorption of 18-crown-6 from aqueous solution on granular activated carbon: a kinetic modeling study, J. Colloid Interface Sci. 299 (2006) 112–115.

[35] Y.H. Chang, K.H. Hsieh, F.C. Chang, Removal of Hg^{2+} from aqueous solution using a novel composite carbon adsorbent, J. Appl. Polym. Sci. 112 (2009) 2445.

[36] M. Auta, B.H. Hameed, Optimized waste tea activated carbon for adsorption of Methylene Blue and Acid Blue 29 dyes using response surface methodology, Chem. Eng. J. 175 (2011) 233.

[37] S. Lagergren, B.K. Svenska, On the theory of so-called adsorption of dissolved substances, R. Swed. Acad. Sci, Doc., Band 24 (1898) 1.

[38] Y.S. Ho, G. McKay, Pseudo-second order model for sorption processes, Process Biochem. 34 (1999) 451.

[39] M. Hasan, A.L. Ahmad, B.H. Hameed, Adsorption of reactive dye onto cross-linked chitosan/oil palm ash composite beads, Chem. Eng. J. 136 (2008) 164.

[40] L. Zhou, Z. Liu, J. Liu, Q. Huang, Adsorption of Hg(II) from aqueous solution by ethylenediamine-modified magnetic crosslinking chitosan microspheres, Desalination 258 (2010) 41.

[41] Y.T. Zhou, C. Branford-White, H.L. Nie, L.M. Zhu, Adsorption mechanism of Cu^{2+} from aqueous solution by chitosan-coated magnetic nanoparticles modified with α-ketoglutaric acid, Colloids Surf. B: Biointerfaces 74 (2009) 244.

[42] N.M. Mahmoodi, B. Hayati, M. Arami, C. Lan, Adsorption of textile dyes on Pine Cone from colored wastewater: kinetic, equilibrium and thermodynamic studies, Desalination 268 (2011) 117.

[43] I.A.W Tan, A.L. Ahmad, B.H. Hameed, Adsorption of basic dye using activated carbon prepared from oil palm shell: batch and fixed bed studies, Desalination 225 (2008) 13.

[44] A.A. Ahmad, B.H. Hameed, Fixed-bed adsorption of reactive azo dye onto granular activated carbon prepared from waste, J. Hazard. Mater. 175 (2010) 298.